

Study of Cu²⁺, Ni²⁺, and Zn²⁺ competitive adsorption on synthetic zeolite: an experimental and theoretical approach

Antonia Mayza de Morais França^a, Francisco Wagner Sousa^b, Adonay Rodrigues Loiola^c, Francisco Murilo Tavares de Luna^d, Carla Bastos Vidal^e, Ronaldo Ferreira do Nascimento^{a,*}

^aDepartment of Analytical Chemistry and Physical Chemistry, Federal University of Ceara, Pici Campus, 60440-900 Fortaleza, CE, Brazil, Tel. +55 85 3366-9958; email: ronaldo@ufc.br (R.F. do Nascimento), Tel. +55 85 3366-9042; mayzauece@gmail.com (A.M. de Morais França)

^bFederal Institute of Education Science and Technology of Ceara - Campus Caucaia, Caucaia-CE, 61642-000, Brazil, Tel. +55 85 3387-1450; email: fr.wagner@gmail.com (F.W. de Sousa)

^cDepartment of Organic and Inorganic Chemistry, Federal University of Ceara, Pici Campus, Fortaleza-CE, 60440-900, Brazil, Tel. +55 85 3366-9972; email: adonay@ufc.br (A.R. Loiola)

^dDepartment of Chemical Engineering, Federal University of Ceara, Pici Campus, Fortaleza-CE, 60440-900, Brazil, Tel. +55 85 3217-1662; email: murilo@gpsa.ufc.br (F.M.T. de Luna)

^eDepartment of Chemistry and Biology, Federal University of Technology - Paraná, Deputado Heitor de Alencar Furtado St., 5000 Ecoville, 81280-340, Curitiba, Paraná, Brazil, Tel. +55 85 3366-9042; email: cvidal@utfpr.edu.br (C.B. Vidal)

Received 14 December 2020; Accepted 20 March 2021

ABSTRACT

In this study, isotherm models were used to describe the interactions between adsorbent (zeolite 4A) and adsorbate (Cu²⁺, Ni²⁺, and Zn²⁺) at different concentrations in both simple and multicomponent systems. To assess the effect of the mass transfer parameters on the adsorption kinetics, the pore diffusivity model was also applied. The adsorption selectivity of the adsorbent material was evaluated as a function of the initial concentration in binary and ternary systems, as well as the competitive adsorption between the metallic ions in synthetic zeolite 4A. The synthesized zeolite was characterized by different techniques such as powder X-ray diffraction, infrared vibrational spectroscopy, and scanning electron microscopy. Langmuir, Freundlich and Sips isotherm models fitted the experimental data of Cu²⁺ and Ni²⁺, whereas Langmuir and Freundlich models fitted the experimental data of Zn²⁺. The adsorption kinetics was fast for Cu²⁺ and Zn²⁺, and slow for Ni²⁺, which is consistent with the pore diffusivity results, in which higher diffusion values for Cu²⁺ and Zn²⁺ were obtained, and indicates a higher selectivity of the synthesized zeolite 4A for Cu²⁺ and Zn²⁺.

Keywords: Zeolite; Metals; Selective adsorption; Isotherm models; Kinetic models

1. Introduction

Wastewater from various anthropogenic activities, whether industrial or domestic, is a worrying source of

environmental pollution due to the high levels of toxic substances [1,2]. Depending on the industrial activity, these effluents might present a large diversity of chemical pollutants. Among the monitored water pollutants, toxic metal ions such as Cu²⁺, Ni²⁺, and Zn²⁺ are widely found in

* Corresponding author.

aquatic systems and soils [3]. These pollutants are reported as harmful to the environment and are related to various human health problems, including cancer, organ damage, and nervous system diseases [4,5].

Several technologies have been used for removing toxic metal ions from aqueous systems. The most important are reverse osmosis, ion exchange, chemical precipitation, electrodialysis, and adsorption [6,7]. However, these technologies present several limitations associated with the high costs of operation, implementation, and reuse [8,9]. In this context, due to the low cost, versatility, simplicity, and high efficiency, the adsorption process is a promising alternative [10–13]. A variety of natural adsorbents, for example, green coconut shell [14,15], sugar cane bagasse [16], and natural clays [17] have been applied to the removal of different classes of pollutants [6]. On the other hand, due to their uniformity in composition and chemical stability, the use of synthetic adsorbents such as zeolites [4,18], alumina [19], and metal oxides [20] to the removal of pollutants, particularly toxic metal ions from aqueous solutions, offers important advantages compared to the natural adsorbents [21,22].

In this sense, zeolites are considered unique adsorbents for the removal of toxic metal ions, given their stable structure, high porosity, high surface area, pore uniformity, availability, and low cost [23], which also favors other application such as catalysis, separation processes, and purification of chemical species, among others [24–26]. Zeolites are defined as hydrated porous aluminosilicates with a crystalline structure and open-chain forms. They comprise a three-dimensional network of SiO_4 and AlO_4^- tetrahedra, linked together by oxygen atoms [27].

The efficiency of zeolites 4A for the adsorption of metals ions in an aqueous medium, in single systems, has been widely reported [28–30]. Multicomponent systems, on the other hand, are more consistent with the complexity found in real samples, allowing a better understanding of the mechanisms involved in the adsorption processes [31]. However, many important issues remain unexplored [10]. In this study, we investigate the selectivity of Cu^{2+} , Ni^{2+} , and Zn^{2+} in binary and ternary systems using zeolite 4A.

2. Materials and methods

2.1. Synthesis of zeolite 4A

Zeolite 4A was synthesized based on the method described by Thompson and Huber [31]. Initially, in a polypropylene beaker, 7.16 g of sodium metasilicate (Na_2SiO_3) was dissolved in 35 mL of NaOH 0.21 mol L^{-1} and, in a separate beaker, 5.00 g of NaAlO_2 was dissolved in 35 mL of NaOH 0.21 mol L^{-1} . The Na_2SiO_3 solution was then added to the NaAlO_2 solution, forming a white thick gel. The solution formed was subjected to magnetic stirring until complete homogenization and then was transferred to a Teflon-lined stainless steel autoclave. The reaction mixture was kept under static conditions at room temperature for 18 h for aging, and then heated at 100°C for 4 h. After cooling, the obtained powder was washed several times with distilled water until reaching a constant pH, and finally dried at 70°C overnight.

2.2. Characterization

The characterization of zeolite 4A was performed to obtain information on its structural and spectroscopic properties. For this, the following techniques were used: X-ray diffraction (XRD), thermogravimetry, Fourier-transform infrared spectroscopy (FTIR), scanning electron microscopy (SEM), and cation exchange capacity (CEC) determination.

2.2.1. X-ray diffraction

XRD measurements were performed using a PANalytical (X-Pert) X-ray powder diffractometer in a Bragg-Brentano geometry. The powder patterns were collected in continuous mode with a 2θ scan speed of 0.5 min^{-1} . $\text{Cu-K}\alpha$ ($\lambda = 1.54 \text{ \AA}$) radiation was used, with tube operating at 40 kV and 25 mA. For these measurements, samples with particle sizes below 74 μm (400 mesh) were selected.

2.2.2. Thermogravimetric analysis

Thermogravimetric analysis was performed using a Shimadzu model TGA-60 H equipment, at a temperature range from 25 to $1,000^\circ\text{C}$, with a heating rate of $10^\circ\text{C min}^{-1}$, in a synthetic air atmosphere (40 mL min^{-1}).

2.2.3. Fourier-transform infrared spectroscopy

Infrared absorption spectra of synthesized zeolite 4A and commercial zeolite 4A were obtained using the PerkinElmer spectrometer, model FTIR SPECTRUM, in the $400\text{--}4,000 \text{ cm}^{-1}$ region. For these experiments, the samples were prepared in a KBr (3 wt.%) wafer.

2.2.4. Scanning electron microscopy

Information about the morphology of zeolite 4A was obtained using an electronic microscope FEG, model Quanta 450, coupled with energy dispersive X-ray analysis. The sample, with a particle size of 200 mesh, was prepared onto a carbon double-sided tape on aluminum support and coated with a thin layer of gold.

2.2.5. Cation exchange capacity

Zeolite 4A was submitted to cation exchange with ammonium ion, following the method described by Vidal et al. [18]. Briefly, 1.00 g of zeolite 4A was added to 10 mL of 10% (w/v) ammonium chloride solution and stirred for 8 h. The system was maintained under static conditions for 16 h. After centrifugation for 5 min at 5,000 rpm, the supernatant was washed 5 times with distilled water to remove ammonium chloride excess. The total nitrogen retained on zeolite 4A through the cation exchange process was determined by the Kjeldahl method.

2.3. Adsorption studies

For all the adsorption experiments, the working solutions of the metal ions were prepared using nitrate salts,

Cu(NO₃)₂·3H₂O, Ni(NO₃)₂·6H₂O, and Zn(NO₃)₂·6H₂O, at pH 5. This pH was chosen to avoid the precipitation of metal ions [32,33].

The Cu²⁺, Ni²⁺, and Zn²⁺ concentrations were determined by the external standard method, using Flame Atomic Absorption Spectrometer (FAAS) model VARIAN 24ZOF5, with an air/acetylene flame and appropriate multi-component hollow cathode lamps (HCL). The wavelength used for Cu²⁺, Ni²⁺, and Zn²⁺ were 324.8, 232.0 and 213.9 nm, respectively.

2.3.1. Dosage effect

Erlenmeyer flasks containing different amounts of zeolite 4A (200 mesh size) were placed in contact with 50 mL of 200 mg L⁻¹ multicomponent solution of Cu²⁺, Ni²⁺, and Zn²⁺ and kept under stirring at 250 rpm for 6 h at room temperature (28°C ± 2°C).

2.3.2. Contact time

125 mL Erlenmeyer flasks containing 0.5 g of zeolite 4A (200 mesh size) were placed in contact with 50 mL of 10, 100, and 200 mg L⁻¹ multicomponent solution (Cu²⁺, Ni²⁺, and Zn²⁺) at pH 5.0 and under stirring at 250 rpm, at room temperature (28°C ± 2°C). At predetermined intervals, aliquots were removed, filtered, and analyzed by FAAS.

2.3.3. Isotherm modeling

Adsorption isotherms were performed using 50.0 mL of single and multi-component solutions (10–1000 mg L⁻¹) at pH 5, and 0.5 g of adsorbent. The systems were submitted to stirring at 250 rpm for 2 h until equilibrium, at room temperature (28°C ± 2°C). Finally, the material was filtered, and the residual concentration was analyzed by FAAS. All experiments were performed in duplicates. The adsorption capacities were calculated using Eq. (1) [34–37]:

$$Q_e = \frac{(C_0 - C_e)}{m_a} V \tag{1}$$

where Q_e (mg g⁻¹) is the equilibrium adsorption capacity, C₀ (mg L⁻¹) is the initial concentration of the metal ion, C_e (mg L⁻¹) is the equilibrium concentration of metal ion, V (L) is the volume of the solution, and m_a (g) is the adsorbent mass.

Equilibrium data obtained were evaluated using the following nonlinearized isotherm models:

Langmuir model [38]

$$Q_e^* = \frac{Q_{\max} k_L C_e}{1 + K_L C_e} \tag{2}$$

where Q_e (mg g⁻¹) is the amount of adsorbed solute per gram of adsorbent at equilibrium, K_L (L mg⁻¹) is the adsorbent and adsorbent interaction constant, Q_{max} (mg g⁻¹) is the maximum adsorption capacity, and C_e (mg L⁻¹) is the concentration of adsorbate at equilibrium.

Freundlich model [39]

$$Q_e = k_f C_e^{1/n} \tag{3}$$

where Q_e (mg g⁻¹) is the amount of solute adsorbed, k_f (mg g⁻¹)(mg L⁻¹)^{1/n} is Freundlich adsorption capacity constant, C_e (mg L⁻¹) is the equilibrium concentration in solution and 1/n is a constant related to surface heterogeneity.

Sips model [40]

$$Q_e = \frac{Q_{\max S} (k_s C_e)^{1/n}}{1 + (k_s C_e)^{1/n}} \tag{4}$$

where Q_e (mg g⁻¹) is the amount of solute adsorbed, Q_{maxS} (mg g⁻¹) is the maximum adsorption capacity, k_s (L mg⁻¹) is the Sips equilibrium constant, C_e (mg L⁻¹) is the equilibrium concentration in solution and n_s represents the degree of system heterogeneity.

Extended Langmuir model [41]

$$Q_e = \frac{Q_{\max} k_i C_i}{1 + \sum_{j=1}^n k_j C_j} \tag{5}$$

where C_i and C_j are the equilibrium concentrations of metals in the multicomponent solution, Q_{max} and k_i are the constants obtained by the Langmuir model applied to the single system, and Q_e is the adsorption capacity at equilibrium.

2.3.4. Kinetic modeling

The adsorption kinetic study was performed using the data obtained from the contact time study. The diffusivity model was applied considering the mass balance in the solid phase and fluid phase [42]. Eqs. (6)–(12) were used to determine the kinetic parameters [43,44]:

Solid phase mass balance

$$\epsilon_p \frac{\partial C_p}{\partial t} + \rho_{ap} \frac{\partial q_i^*}{\partial t} = D_p \epsilon_p \left(\frac{\partial^2 C_p}{\partial r^2} + \frac{2}{r} \frac{\partial C_p}{\partial r} \right) \tag{6}$$

Initial conditions

$$t = 0, C_p = C_0, C_b = 0, q = 0 \tag{7}$$

Boundary conditions

$$r = 0, \frac{\partial C_p}{\partial r} = 0 \tag{8}$$

$$r = R_p, D_p \epsilon_p \frac{\partial C_p}{\partial r} = k_f (C_b - C_p) \tag{9}$$

Mass balance in the liquid phase

$$r = R_p \frac{dC_b}{dt} = -\frac{3V_a k_f}{RV_l} \left(C_b - C_p \Big|_{r=R_p} \right) \quad (10)$$

Initial conditions

$$t = 0, C_b = C_0 \quad (11)$$

where C_b is the bulk liquid phase concentration, C_p is the intra-particle liquid phase concentration, q_i^* is the amount of metal retained by the adsorbent [Eq. (2)], ε_p is the porosity of the particle (zeolite 4A), V_a is the volume of the adsorbent, V_l is the volume of the liquid, R_p is the particle radius of zeolite 4A, D_p is the pore diffusivity coefficient, k_f is the external coefficient of mass transfer, t is the time and r is the radial coordinate.

The kinetic parameters were calculated using the simulator gPROMS, which is composed of systems of differential equations and partial algebraic. The radial domain was discretized using a third-order orthogonal collocation method in finite elements. The mass transfer parameter (D_p) was obtained using an optimization package employing the heteroscedastic method (gPROMS User Guide v3.2.0, 2009) [45].

According to the dimensional analysis, the mass transfer coefficient (or diffusion coefficient) (k_f) can be determined using the correlation based on Sherwood (Sh), Schmidt (Sc), and Reynolds (Re) numbers, which is valid for isolated spheres. Thus, k_f was calculated from the following correlation for small particles [46].

$$\text{Sh} = 2 + 0.6\text{Re}^{1/2} \text{Sc}^{1/3} \quad (12)$$

$$\text{Sh} = \frac{k_f d_p}{D_m} \quad (13)$$

$$\text{Sc} = \frac{\nu}{D_m} \quad (14)$$

$$\text{Re} = \frac{\nu d_p}{\nu} \quad (15)$$

where: for container shaking the peripheral velocity is given by:

$$\nu = d_{\text{imp}} N^* \quad (16)$$

where D_p (m) is particle diameter, d_{imp} (m) is impeller diameter, ν ($\text{m}^2 \text{s}^{-1}$) is fluid kinematic viscosity, ν (m s^{-1}) is impeller peripheral velocity, D_m (m s^{-1}) is metal diffusivity in water and N^* (rpm) is impeller speed.

The fit of the model to the experimental data was evaluated by applying the root mean square error (RMSE) equation, as shown in Eq. (17).

$$\text{RMSE} = \sqrt{\frac{1}{N} \sum_{i=1}^N (C_{\text{Sim}} - C_{\text{Exp}})^2} \quad (17)$$

where C_{Sim} is the estimated concentration from the model, C_{Exp} is the experimental concentration, and N is the number of measured values. Small RMSE values indicate a better fit of the model to the experimental data.

2.3.5. Selectivity

The selectivity (S) was calculated in binary and ternary systems at different concentrations using, respectively, Eqs. (18) and (19) [47].

$$S = \frac{(Q/C_e)_a}{(Q/C_e)_b} \quad (18)$$

$$S = \frac{(Q/C_e)_a}{(Q/C_e)_b + (Q/C_e)_c} \quad (19)$$

where Q is the concentration of adsorbate in adsorbent (mg g^{-1}) and C_e is the adsorbate concentration at equilibrium (mg L^{-1}).

2.3.6. Competitive adsorption

Competitive adsorption usually occurs in multicomponent systems, and three main possible types of effects occur: synergism, antagonism, and noninteraction [48]. The interactive effect of each ion metal was evaluated by the maximum adsorption capacities, calculated by means of the Langmuir model, with or without the coexistence of other metal ions in the medium, using the following relation:

$$\frac{Q_{\text{max}}^{\text{min}}}{Q_{\text{max}}^0} \quad (20)$$

where Q_{max}^0 is the maximum adsorption for a single system and $Q_{\text{max}}^{\text{mix}}$ is the maximum adsorption capacity of the multicomponent system, which can be found in Tables 3 and 7, respectively. Thus, if $Q_{\text{max}}^{\text{mix}}/Q_{\text{max}}^0 > 1$, then the adsorption is promoted by the presence of other metal ions (synergistic effect); if $Q_{\text{max}}^{\text{mix}}/Q_{\text{max}}^0 = 1$, then there is no observed interaction; and if $Q_{\text{max}}^{\text{mix}}/Q_{\text{max}}^0 < 1$, then the adsorption is suppressed by the presence of other metal ions in the medium (antagonistic effect) [49].

After determining the type of interaction in the system, the rate of adsorption reduction was calculated using Eq. (21) [50].

$$\Delta Y = \frac{Q_{\max}^0 - Q_{\max}^{\text{mix}}}{Q_{\max}^{\text{mix}}} \times 100 \quad (21)$$

where ΔY corresponds to the rate of adsorption reduction.

3. Results and discussion

3.1. Zeolite 4A characterization

3.1.1. X-ray diffraction

The X-ray pattern of the synthesized zeolite (Fig. 1a) shows good agreement in terms of both peaks location and intensity, compared to the XRD pattern of a commercial zeolite (Fig. 1b). In addition, as shown by the peak identification using the ICSD 35119 database, zeolite 4A was identified as a single crystalline phase, free of impurities [51].

3.1.2. Thermogravimetric analysis

The thermogravimetry profile for sample zeolite 4A (Fig. 2) showed two thermal events, at 194°C and at 348°C, which may be associated with the loss of both free and

physically adsorbed water within zeolite pores. However, the temperature difference between them suggests that the interaction of water with the zeolite 4A structure occurs in a nonuniform manner. In addition, the observed weight loss was around 20% at 400°C, which is consistent with water release due to condensation of vicinal silanol groups, as described in the work of Musyoka et al. [52].

3.1.3. Fourier-transform infrared spectroscopy

Characteristic absorption bands of zeolite 4A are observed by FTIR for the synthesized zeolite (Fig. 3a) and for the commercial zeolite (Fig. 3b). The band at 464 cm^{-1} is attributed to the deformation internal vibration of the T(Si, Al)–O bond, which corresponds to a four-membered double ring (D4-R). At 558 cm^{-1} , a band referring to the external vibration of the D4-R can be observed. The band at 665 cm^{-1} is attributed to the internal vibrations of symmetrical stretching of the T(Si, Al)–O bonds. The band at 1,005 cm^{-1} is attributed to the internal vibrations of the asymmetric stretching of the T (Si,Al)–O bonds, and the band at 1,656 cm^{-1} refers to the angular deformation of the hydroxyl group present

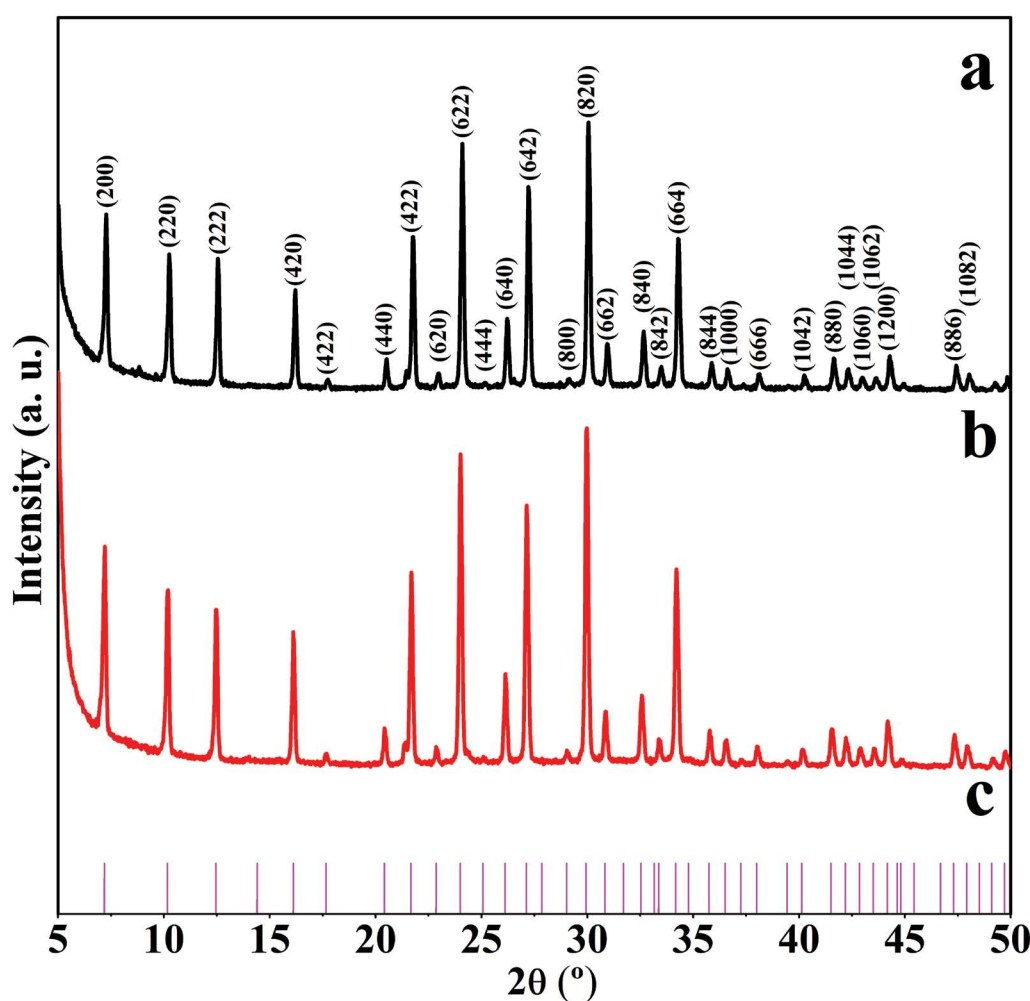


Fig. 1. X-ray patterns for (a) synthesized zeolite 4A, (b) commercial zeolite 4A and (c) zeolite 4A standard.

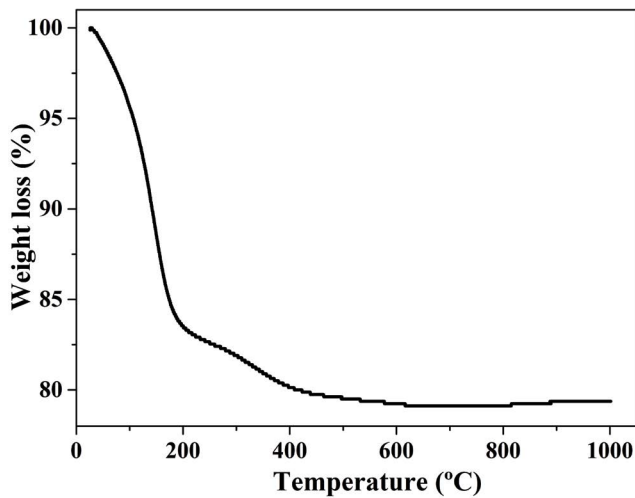


Fig. 2. Thermogravimetric curve of zeolite 4A in synthetic air atmosphere and a heating rate of $40^{\circ}\text{C min}^{-1}$.

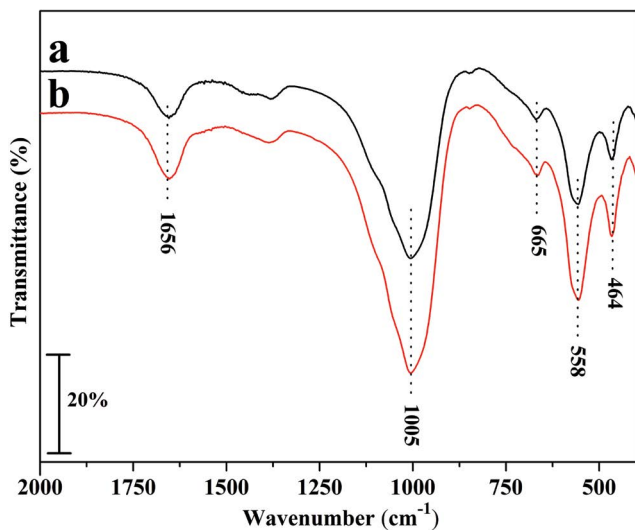


Fig. 3. Infrared spectra for (a) zeolite 4A and (b) commercial zeolite.

in the water molecules. Similar results have been reported concerning FTIR studies of zeolite 4A [53–55].

3.1.4. Scanning electron microscopy

Zeolite 4A micrographs obtained by SEM are presented in Fig. 4. The synthesized zeolite 4A shows uniform particle size, which can be clearly observed by the presence of particles with ca. $1\ \mu\text{m}$ and with cubic habit, characteristic of zeolite 4A [27]. In the micrograph with the highest magnification, it is possible to observe that the formed grains have smooth faces, with some cubic crystal intergrowths.

3.1.5. Cation exchange capacity

The CEC indicated that part of the Na^+ present in the zeolite 4A sample ($\text{Na}_{12}\text{Si}_{12}\text{Al}_{12}\text{O}_{48}\cdot 27\text{H}_2\text{O}$) was replaced by NH_4^+ . The CEC value was $188\ \text{mmol NH}_4^+$

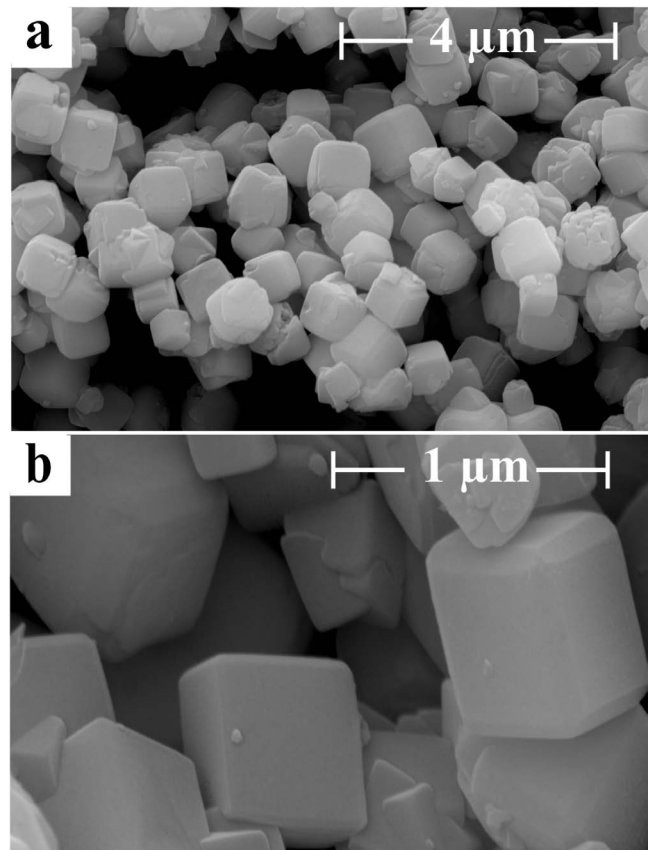


Fig. 4. Zeolite 4A micrographs with different magnifications.

$100\ \text{g}^{-1}$ adsorbent. This value corresponds to 34% when compared to the total theoretical value of $547\ \text{mmol (NH}_4^+ 100\ \text{g}^{-1})$, which was calculated based on the zeolite 4A unit cell chemical formula. However, the results obtained are consistent with the CEC ($251.6\ \text{mmol NH}_4^+ 100\ \text{g}^{-1}$) reported by Ren et al. [56] using a commercial zeolite A.

3.2. Adsorption experiments

The adsorption phenomenon can be influenced by several physical-chemical factors in which adsorbent dosage, contact time, initial concentration, and pH play major roles [57–59]. In this study, we evaluated the influence of adsorbent dosage (zeolite 4A), contact time, and initial concentration on the adsorption of Cu^{2+} , Ni^{2+} , and Zn^{2+} . Given the fact that $\text{pH} \approx 5$ is a consolidated value in metal ion adsorption studies using zeolite, this value was used for all the adsorption experiments. Some studies report that at this pH the metal ions adsorption is favored due to the dissociation of hydroxyl groups, contributing to the increase of anionic sites [60]. Furthermore, at high pH (>6), the solubility of the ions decreases, favoring precipitation and, consequently, hindering the adsorption process [32].

3.2.1. Dosage effect

The minimum amount of the adsorbent required for maximum metal ions removal is shown in Fig. 5. Cu^{2+} and Zn^{2+} removals were 80% ($4\ \text{g L}^{-1}$ dosage) and 99% ($10\ \text{g L}^{-1}$ dosage), respectively. For Ni^{2+} , removals of 40%,

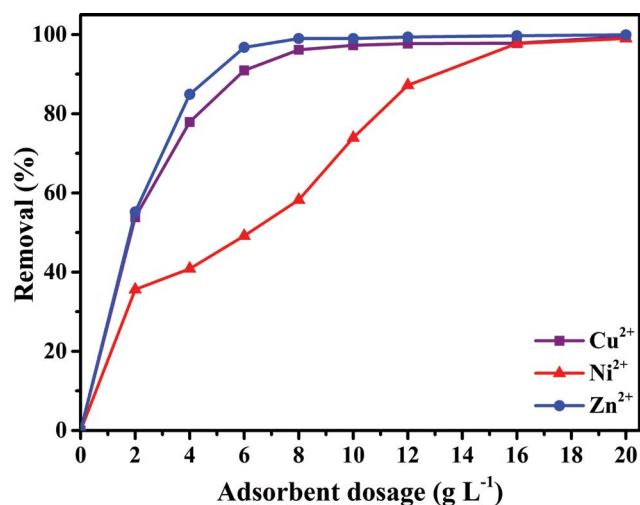


Fig. 5. Percentage of metal ion removal using different adsorbent contents, 200 mg L⁻¹ concentration, pH 5.0, multicomponent solution, and 6 h contact time.

74% and 97% were obtained for dosages of 4, 10, and 16 g L⁻¹, respectively. The increase in the removal of metal ions with the increase in dosage is possibly related to the increase in the number of active sites, porosity, and the increase in the material surface area [61,62]. The dosage of 10 g L⁻¹ was chosen for the subsequent batch adsorption experiments.

3.2.2. Contact time

Fig. 6 shows the Cu²⁺, Ni²⁺, and Zn²⁺ removal for concentrations of 10, 100, and 200 mg L⁻¹ of the multicomponent system as a function of contact time between adsorbent–adsorbate. It can be observed in Fig. 6a that the Cu²⁺ and Zn²⁺ removals at 10 mg L⁻¹ reached approximately 100%, in the first 10 min. The Ni²⁺ removal reached approximately 65%. After 120 min, the Ni²⁺ removal was close to 100%. On the other hand, the Cu²⁺, Zn²⁺, and Ni²⁺ removals at 100 mg L⁻¹ multicomponent solution (Fig. 6b) were 99%, 99%, and 40%, respectively, obtained at 10 min. For 200 mg L⁻¹ the removals were 91%, 91%, and 27%, for Cu²⁺, Zn²⁺, and Ni²⁺, respectively.

The reduction in the removal of metal ions with the increase of their concentrations is probably due to the effect of competition for the active sites available in the material and by the electrostatic interaction [63]. For further studies of the adsorption isotherms, a contact time of 120 min was chosen.

Additionally, considering the initial concentration of 200 mg L⁻¹, the Na⁺ exchanged for the total amount of metal ions adsorbed was estimated at approximately 23%, which is in line with the value reported by Hui et al. [60]. The removal of metal ions in zeolite 4A can be associated with a mechanism involving processes of both adsorption and ion exchange [64].

3.2.3. Adsorption isotherm

The adsorption isotherms obtained for single and multicomponent systems are shown in Fig. 7. For low

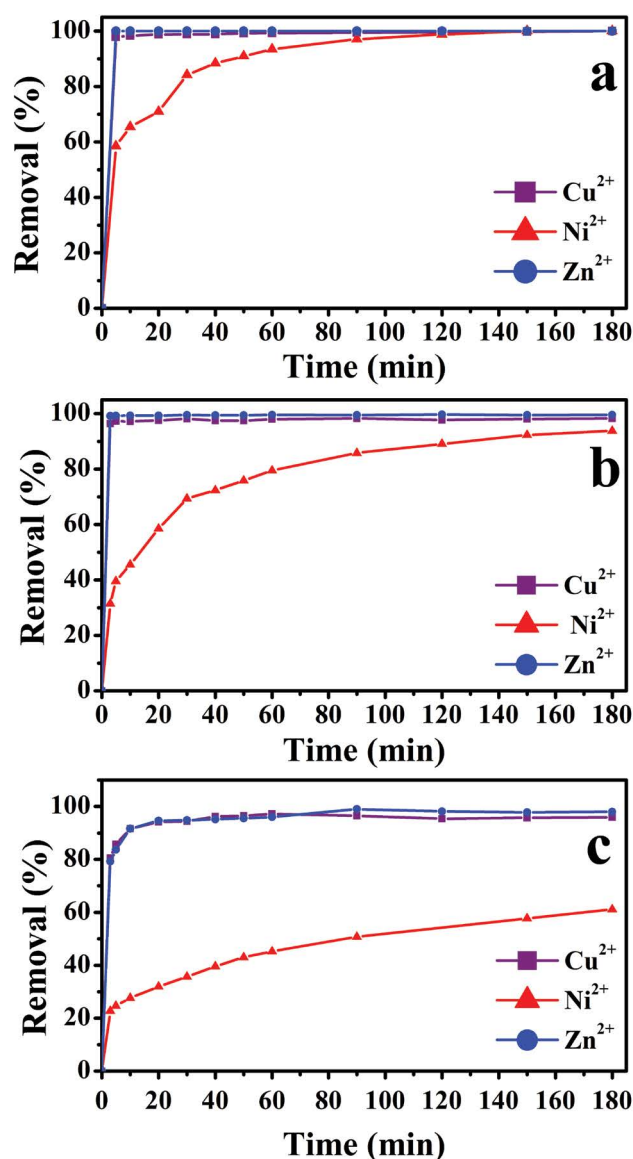


Fig. 6. Contact time for Cu²⁺, Ni²⁺, and Zn²⁺ for multicomponent solutions in different concentrations: (a) 10 mg L⁻¹, (b) 100 mg L⁻¹ and (c) 200 mg L⁻¹. (200 mesh particle size, pH 5.0 and 10 g L⁻¹ dosage of zeolite 4A).

concentrations (Cu²⁺, Ni²⁺, and Zn²⁺), the behavior and the magnitudes of adsorption capacity are similar in both systems. However, for high metal ions concentrations, the adsorption capacities were higher for the single system than for the multicomponent one, suggesting strong competition at the highest concentrations. The obtained orders for adsorption capacity (in mg g⁻¹), for the single and multicomponent systems, were respectively: Zn (79.27) > Cu (70.22) > Ni (37.43) and Cu (58.00) > Zn (56.06) > Ni (25.46).

Experimental data for Cu²⁺, Ni²⁺, and Zn²⁺ are shown in Fig. 8 together with the Langmuir, Freundlich, and Sips isotherms model adjustments. Table 2 shows the constants values from the models, calculated by the non-linear model.

The Langmuir model represents the best fit of the experimental data for Cu²⁺ and Zn²⁺ (based on the error

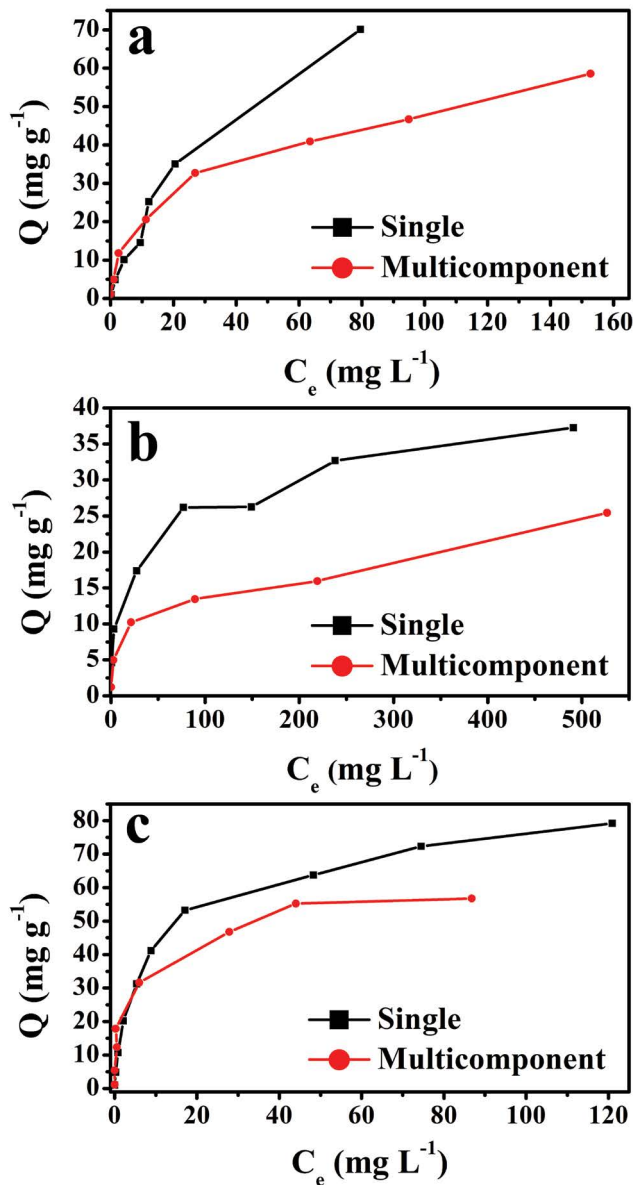


Fig. 7. Comparison between single and multicomponent isotherms: (a) Cu^{2+} , (b) Ni^{2+} , and (c) Zn^{2+} using zeolite 4A. Concentration of 200 mg L^{-1} , 0.5 g adsorbent at pH 5.0.

function and R^2 values), which might suggest a monolayer adsorption mechanism on zeolite 4A surface [65]. The Freundlich model proved more suitable for Ni^{2+} , indicating the presence of adsorption sites with different adsorptive energies [63].

However, analysis of variance (F test) for a 95% confidence level (Table 1) indicated that the Langmuir, Freundlich, and Sips models fitted experimental data for Cu^{2+} and Ni^{2+} ($F_{\text{calculated}} < F_{\text{tabulated}}$). For the Zn^{2+} , no statistical difference is observed ($F_{\text{calculated}} < F_{\text{tabulated}}$) for the fitting of the Langmuir and Freundlich models. The contrary was observed for the Sips model in comparison with Freundlich and Langmuir models. ($F_{\text{calculated}} > F_{\text{tabulated}}$).

As shown in Table 2, the high values of maximum adsorption capacity for Cu^{2+} and Zn^{2+} are in conformity with

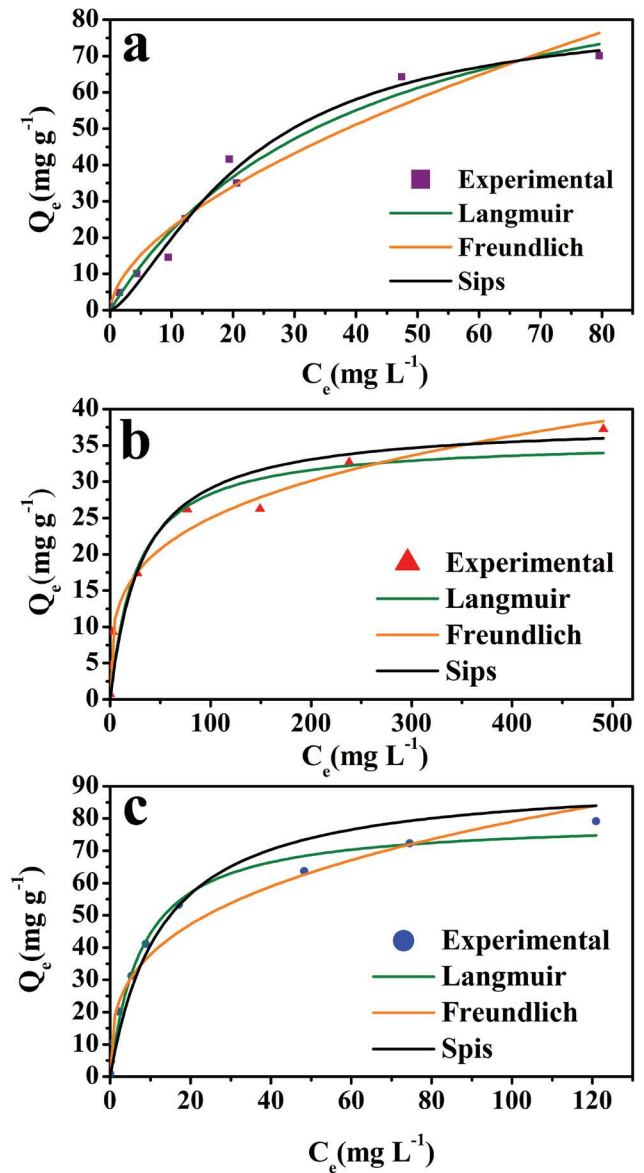


Fig. 8. Experimental and theoretical adsorption isotherms of ions (a) Cu^{2+} , (b) Ni^{2+} , and (c) Zn^{2+} on zeolite 4A, single system.

Table 1
Analysis of variance for the three isothermal models

	Cu^{2+}	Ni^{2+}	Zn^{2+}	
	F_{cal}	F_{cal}	F_{cal}	F_{tab}
Langmuir/Freundlich	0.208	0.027	0.437	3.889
Langmuir/Sips	0.063	2.070	4.295	3.889
Freundlich/Sips	0.489	1.408	6.356	3.889

the Langmuir and Sips models, whereas low capacity values were obtained for Ni^{2+} .

This way, the following orders of maximum adsorption capacity were obtained for the Langmuir

and Sips models, respectively: $\text{Cu}^{2+} > \text{Zn}^{2+} > \text{Ni}^{2+}$ and $\text{Zn}^{2+} > \text{Cu}^{2+} > \text{Ni}^{2+}$.

The efficiency of the adsorption process depends both on the characteristics of the zeolite and the nature of the metal ions [60]. Zeolites, in general, are weakly acidic and, therefore, exchangers in sodium form are selective for hydrogen. This contributes to raising the pH of the solution and enables the formation of metal hydroxide [66]. The characteristics of metal ions such as ionic radius, hydrolysis constant, dehydration energy, and hydrated radius, are summarized in Table 3.

According to the data in Table 3, the following selectivity sequences are expected: $\text{Ni}^{2+} > \text{Cu}^{2+} > \text{Zn}^{2+}$, $\text{Zn}^{2+} > \text{Cu}^{2+} > \text{Ni}^{2+}$ and $\text{Cu}^{2+} > \text{Zn}^{2+} > \text{Ni}^{2+}$, considering hydration radius, hydration energy, and hydrolysis constant, respectively [67–69]. Therefore, it is suggested that the selectivity sequence obtained from the hydration energy and the hydrolysis constant are consistent with the Q_{max} sequences obtained by the Langmuir and Sips models, respectively. As a consequence, they can both be considered critical parameters that affected the metal ions adsorption. It is reported that the hydration

energy of metal ions is one of the factors of high influence on the adsorption capacity of zeolite 4A [70,71]. Metal ions with greater hydration energy and hydrolysis constant are preferred to remain in the solution phase because of the strong interaction with water molecules [67]. Nonetheless, the hydrolysis constant of metal ions depends on the type of metal hydrolysis (MOH^+) [72], since the cationic complexes can be more strongly adsorbed than free metal cations. This behavior is expected to occur due to the formation of metal hydroxide complexes, which are thermodynamically more stable and easier to be adsorbed than the free metal ion [73,74].

Table 4 presents a comparison of the maximum adsorption capacity with the values reported in the literature for commercial zeolite and zeolite 4A prepared from coal fly ash.

3.2.4. Kinetic modeling

The kinetic diffusivity model was applied to estimate the diffusion of Cu^{2+} , Ni^{2+} , and Zn^{2+} on zeolite 4A, as shown in Fig. 9 and Table 5. It can be observed that the

Table 2

Model parameters obtained of the adsorption isotherms with the zeolite 4A for (Cu^{2+} , Ni^{2+} , and Zn^{2+}) single system

		Cu^{2+}	Ni^{2+}	Zn^{2+}
Langmuir	Q_{exp}	70.140	37.260	79.170
	Q_{max}	110.126 ± 12.214	35.777 ± 3.135	79.642 ± 2.440
	K_L	0.025 ± 0.005	0.037 ± 0.016	0.126 ± 0.014
	R^2	0.974	0.929	0.988
	AIC	28.718	24.440	25.442
	SQE	112.336	76.285	71.904
	HYBRID	4.752	8.354	4.194
	N	1.714 ± 0.203	3.710 ± 0.302	3.121 ± 0.289
Freundlich	k_f	5.942 ± 1.556	7.219 ± 0.835	18.072 ± 2.133
	R^2	0.945	0.984	0.967
	AIC	35.783	12.352	36.467
	SQE	246.266	16.835	216.561
	HYBRID	11.712	1.826	17.540
	Q_{maxS}	82.797 ± 0.010	38.282 ± 6.554	92.903 ± 12.251
Sips	n_s	0.690 ± 0.138	1.000 ± 0.462	1.000 ± 0.261
	k_s	0.045 ± 0.010	0.032 ± 0.017	0.078 ± 0.030
	R^2	0.979	0.906	0.952
	AIC	30.306	30.813	43.223
	SQE	78.611	84.019	277.251
	HYBRID	6.032	8.354	4.194

Akaike's Information Criterion (AIC); Squared Error (SQE); Hybrid Fractional Error (HYBRID).

Table 3

Physicochemical parameters of Cu^{2+} , Ni^{2+} , and Zn^{2+}

Metal ions	Ionic radius (Å)	Hydration radius (Å)	Hydration energy (kJ mol^{-1})	Hydrolysis constant (pK_i)
Zn^{2+}	0.740	4.300	-2,046	8.960
Cu^{2+}	0.720	4.190	-2,100	7.960
Ni^{2+}	0.700	4.040	-2,105	9.860

Table 4
Comparison of maximum adsorption capacities of the synthesized zeolite 4A and with data from literature

Zeolite type	Metal	Initial concentration (mg L ⁻¹)	T (°C)	Q _{max} mg g ⁻¹	pH	Reference
Commercial zeolite 4A	Cu ²⁺	50–300	25 ± 0.5	53.450	3.0	[60]
	Ni ²⁺			7.900		
	Zn ²⁺			31.580		
	Cr ²⁺			45.290		
Coal fly ash prepared zeolite 4A	Cu ²⁺	50–300	25 ± 0.5	50.450	3.0	[60]
	Ni ²⁺			8.960		
	Zn ²⁺			30.800		
	Cr ²⁺			41.610		
Zeolite 4A	Ni ²⁺	10–1,000	28 ± 0.5	61.482	5.0	This study
	Zn ²⁺			55.018		

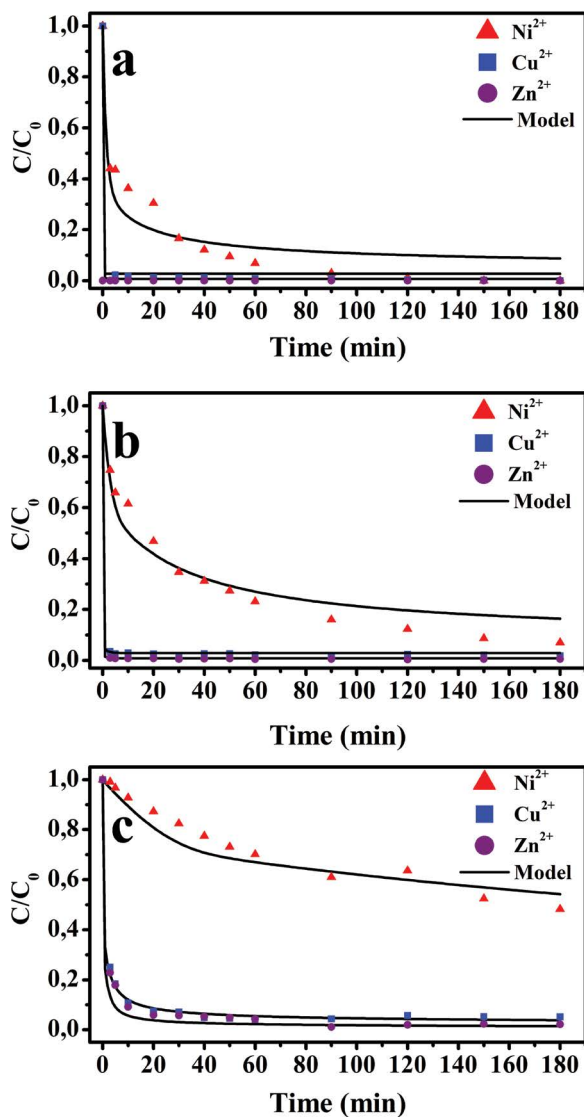


Fig. 9. Experimental and theoretical kinetic curves for Cu²⁺, Ni²⁺, and Zn²⁺ in multicomponent solutions: (a) 10 mg L⁻¹, (b) 100 mg L⁻¹, and (c) 200 mg L⁻¹, using 0.5 g adsorbent at pH 5.0.

calculated values agree with the experimental data, with low RMSE values (<10⁻²). It can also be noted that the metal ion concentration in the liquid phase decreases faster with the decrease of the initial concentration. Gama et al. [75] suggest that this behavior is related to the concentration of metal ions, as well as to the diffusion and adsorption of metal ions in the adsorbent pores. However, for higher concentrations, the removal rate decreases, probably because of the increased competition for the sites.

As it can be observed in Table 5, the increase of the initial metal ions concentrations leads to the decrease of their diffusivity within the pores of zeolite 4A. This occurs in the order of magnitude of 10³, 10³, and 10² for Cu²⁺, Zn²⁺, and Ni²⁺, respectively. A likely explanation for this behavior may be associated with the reduction of available adsorption sites with the increase in the initial concentration of the metal ions [76]. This behavior may also be related to other thermodynamic aspects, as indicated in several studies with similar observations [42,77,78].

In contrast, the diffusion coefficient values were calculated by correcting Sh, Sc and Re [Eqs. (12)–(16)] are completely independent of the initial concentrations (of the ions of interest) and the adsorbent mass [79].

This suggests that, given their high k_f values, Cu²⁺ and Zn²⁺ have greater mobility to break the film surrounding the adsorbent particle [46].

3.2.5. Selectivity

The selectivity study was performed to confirm the preference for metal ion adsorption on zeolite 4A for both binary and ternary systems. Table 6 shows that the selectivity of Cu²⁺ increases with the increase of concentration, whereas the opposite occurs for Zn²⁺, for the ternary and binary systems. This is due to the competition for specific adsorption sites, and implies a decrease in the adsorption of metal ions [48,80].

Zeolite 4A has less selectivity for Ni²⁺ for binary and ternary systems. This result is consistent with those reported in other studies using zeolite 4A [60,81]. For the ternary system, the following order was obtained: Zn²⁺ > Cu²⁺ > Ni²⁺. Known selectivities

for other types of zeolite are: $Pb^{2+} > Zn^{2+} > Cd^{2+} > Cu^{2+}$ for clinoptilolite [82], $Pb^{2+} > Cd^{2+} > Cu^{2+} > Ni^{2+}$ for zeolite 4A [83], $Pb^{2+} > Cu^{2+} > Cd^{2+} > Ni^{2+}$ for zeolite X [83], $Pb^{2+} > Cd^{2+} > Cu^{2+} > Ni^{2+}$ for mordenite [84], and $Cr^{3+} > Cu^{2+} > Zn^{2+} > Cd^{2+} > Ni^{2+}$ for NaP1 [85]. In general, these zeolites show greater preference for Cu^{2+} and Zn^{2+} and less preference for Ni^{2+} . However, such differences might be associated with differences in the properties of the zeolites and the experimental techniques used [66].

3.2.6. Competitive adsorption

The competitive constant for (Cu^{2+} , Ni^{2+} , and Zn^{2+}) binary and ternary adsorption systems were determined, followed by the classification according to the interaction effect (Table 7).

The results of capacity ratio (Q_{max}^{mix}/Q_{max}^0) for Cu^{2+} in the presence of Zn^{2+} are shown in Table 7. A value of 0.233 indicates a decrease of 76.6% in adsorption compared to

Table 5

Coefficient of diffusion (k_f) and pore diffusivity (D_p) as a function of the initial concentration of the multicomponent solution for Cu^{2+} , Ni^{2+} , and Zn^{2+}

Metal ions	Concentration (mg L ⁻¹)	k_f (cm min ⁻¹)	D_p (cm ² min ⁻¹)	RMSE
Cu^{2+}	10	12.937	6.657×10^{-5}	1.827×10^{-4}
	100		5.712×10^{-6}	6.461×10^{-4}
	200		6.643×10^{-8}	2.993×10^{-3}
Ni^{2+}	10	12.320	1.648×10^{-8}	8.253×10^{-4}
	100		4.655×10^{-9}	6.571×10^{-3}
	200		4.063×10^{-10}	9.722×10^{-3}
Zn^{2+}	10	12.738	4.201×10^{-5}	7.431×10^{-5}
	100		1.523×10^{-5}	2.346×10^{-4}
	200		9.847×10^{-8}	8.283×10^{-3}

Table 6

Adsorption selectivity as a function of the initial concentrations of Cu^{2+} , Ni^{2+} , and Zn^{2+} in the ternary and binary system, using 0.5 g adsorbent at pH 5.0

C_0 (mg L ⁻¹)	$(Cu^{2+}/Ni^{2+}/Zn^{2+})$			(Cu^{2+}/Zn^{2+})		(Cu^{2+}/Ni^{2+})		(Ni^{2+}/Zn^{2+})	
	Cu^{2+}	Ni^{2+}	Zn^{2+}	Cu^{2+}	Zn^{2+}	Cu^{2+}	Ni^{2+}	Ni^{2+}	Zn^{2+}
100	0.208	0.018	4.267	0.229	4.365	5.636	0.177	0.151	6.618
200	0.026	0.002	34.844	0.298	3.388	20.238	0.049	0.045	22.359
500	0.383	0.018	2.395	0.577	1.734	184.665	0.005	0.020	51.088
800	5.395	0.051	0.120	1.388	0.720	412.884	0.002	0.038	26.432
1,000	6.084	0.045	0.109	1.520	0.658	132.548	0.008	0.053	18.792

Table 7

Competition and interaction effects of Cu^{2+} , Ni^{2+} , and Zn^{2+} ions in the binary and ternary adsorption systems. Concentration of 200 mg L⁻¹; 0.5 g adsorbent at pH 5.0

Metal	Adsorption systems	Q_{max}^{mix} mg g ⁻¹	Competitive constants		Interaction effect
			Q_{max}^{mix}/Q_{max}^0	$\Delta Y\%$	
Cu^{2+}	Cu^{2+}/Zn^{2+}	25.712	0.233	76.652	Antagonistic
	Cu^{2+}/Ni^{2+}	128.232	1.164	-16.441	Synergistic
	$Cu^{2+}/Ni^{2+}/Zn^{2+}$	61.482	0.558	44.171	Antagonistic
Ni^{2+}	Ni^{2+}/Zn^{2+}	20.216	0.565	43.494	Antagonistic
	Ni^{2+}/Cu^{2+}	18.460	0.516	48.403	Antagonistic
	$Ni^{2+}/Cu^{2+}/Zn^{2+}$	31.733	0.887	11.300	Antagonistic
Zn^{2+}	Zn^{2+}/Ni^{2+}	89.362	1.122	-12.205	Synergistic
	Zn^{2+}/Cu^{2+}	59.064	0.742	25.115	Antagonistic
	$Zn^{2+}/Cu^{2+}/Ni^{2+}$	55.018	0.691	30.918	Antagonistic

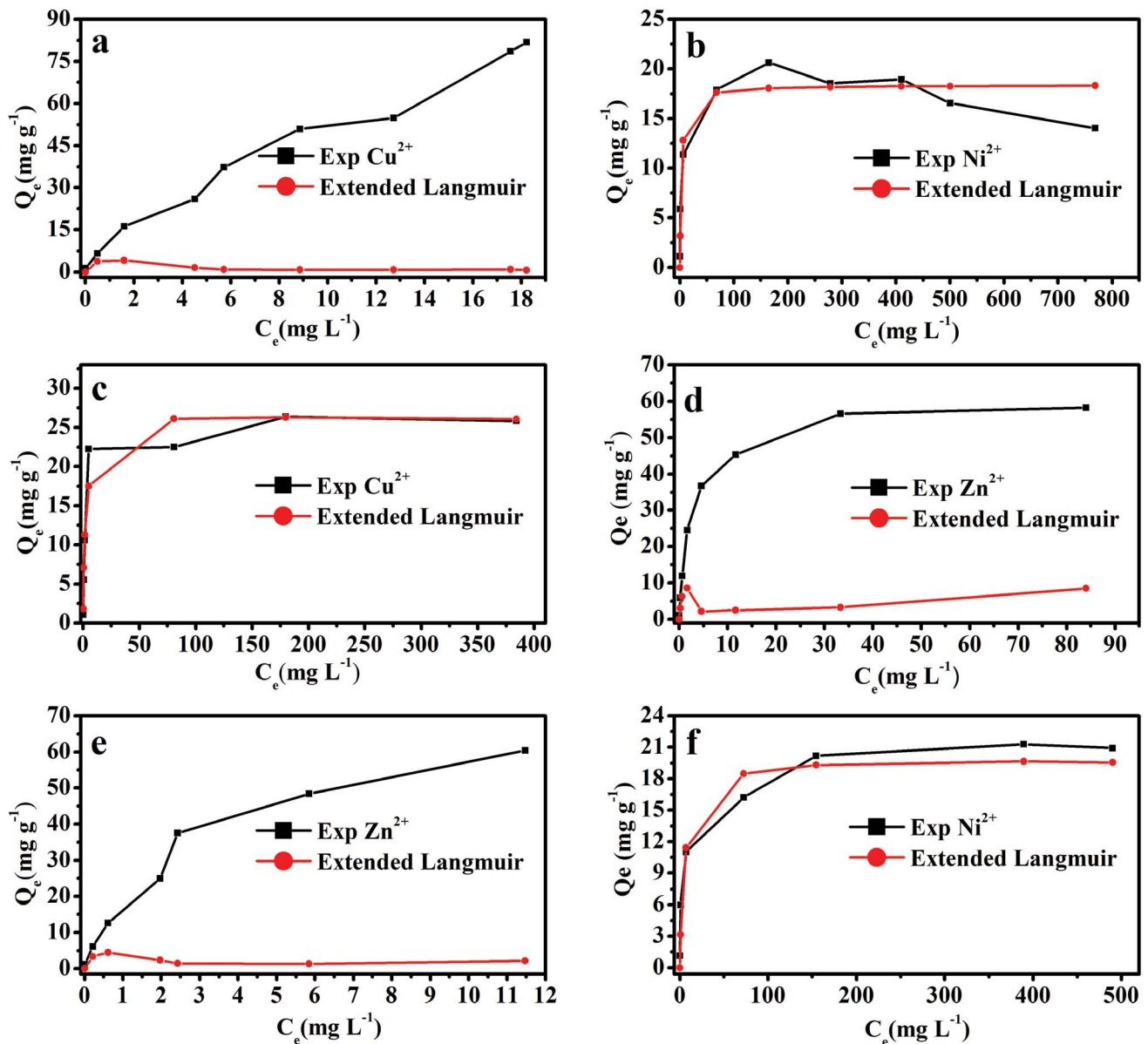


Fig. 10. Adjustment of the extended Langmuir model to the experimental data of the binary systems (a, b) $\text{Cu}^{2+}/\text{Ni}^{2+}$, (c, d) $\text{Cu}^{2+}/\text{Zn}^{2+}$ and (e, f) $\text{Zn}^{2+}/\text{Ni}^{2+}$.

the single system. A similar trend was observed for adsorption of Zn^{2+} in the presence of Cu^{2+} ($Q_{\text{max}}^{\text{mix}}/Q_{\text{max}}^0$ of 0.742), with a reduction in adsorption of 25.1%. These results indicate an antagonistic effect among the metal ions, particularly with Zn^{2+} . Sellaoui et al. [49] obtained a similar result for adsorption of $\text{Pb}^{2+}/\text{Hg}^{2+}$ using a bentonite-alginate composite. For the binary systems ($\text{Cu}^{2+}/\text{Ni}^{2+}$ and $\text{Zn}^{2+}/\text{Ni}^{2+}$), it was found that the presence of Ni^{2+} did not reduce the adsorption capacity. However, it can be suggested that Ni^{2+} favors the increase of Q_{max} for Cu^{2+} and Zn^{2+} . Therefore, it is possible that the Ni^{2+} adsorption sites are different from the ones of Cu^{2+} and Zn^{2+} , showing the synergistic effect between them. In contrast, Cu^{2+} and Zn^{2+} had an antagonistic effect of 0.516 and 0.565, respectively, on Ni^{2+} adsorption. This implies an adsorption reduction of 48.4% and 43.5%,

respectively. The same effect was observed in the ternary system, in which there was a reduction of 44.2% in the adsorption of Cu^{2+} , 30.9% for Zn^{2+} , and 11.3% for Ni^{2+} .

Similar behavior was observed when adjusting the Langmuir model extended to the experimental data of the binary and ternary systems (Figs. 10 and 11). In the combination of $\text{Cu}^{2+}/\text{Ni}^{2+}$ and $\text{Zn}^{2+}/\text{Ni}^{2+}$, the extended model presented better adjustment for the Ni^{2+} experimental data (errors of 4.4 and 3.1), confirming that there is no competition of this ion with the other two for the adsorption sites. Opposite results were found for Cu^{2+} and Zn^{2+} , in which a significant discrepancy between theoretical and experimental data (errors of 100.5 and 61.4, respectively) was observed. This indicates that the extended Langmuir model does not describe the behavior of Cu^{2+} and Zn^{2+} ,

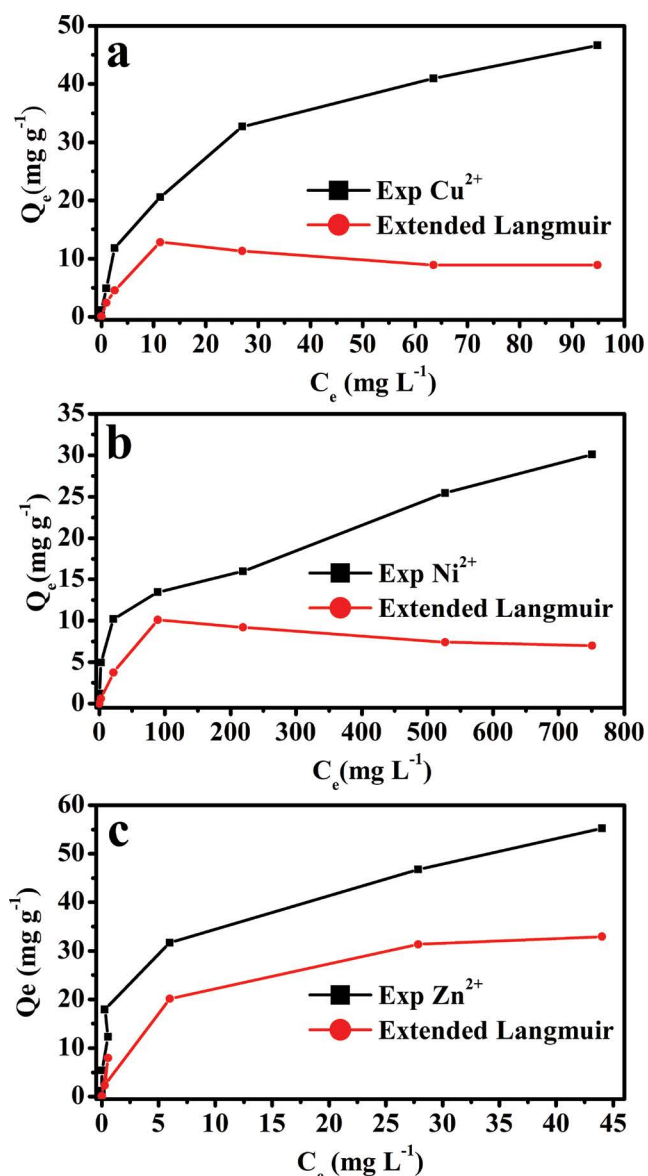


Fig. 11. Adjustment of the extended Langmuir model to the experimental data of the ternary systems (a) Cu^{2+} , (b) Ni^{2+} and (c) Zn^{2+} .

confirming their antagonistic effects on Ni^{2+} adsorption onto zeolite. In addition, the extended model showed a much better adjustment for Cu^{2+} (error 4.8) than for Zn^{2+} (error 45.0), in the $\text{Cu}^{2+}/\text{Zn}^{2+}$ system. Therefore, it is suggested a greater interference of Zn^{2+} in the adsorption of Cu^{2+} than the opposite, corroborating the results reported in Table 7.

Regarding the ternary system, a significant difference was observed between the calculated and experimental data for Cu^{2+} , Ni^{2+} , and Zn^{2+} (error of 38.9, 22.1 and 24.0), indicating that the extended Langmuir model failed to explain the adsorption of the ternary mixture. Thus, the failure of the model suggests a competitive adsorption [86,87].

4. Conclusions

The characterization results of the adsorbent material used showed that the synthesis performed by the hydrothermal method was efficient and led to the formation of zeolite 4A as a single crystalline phase. Adsorption efficiency for single and multicomponent system, were respectively $\text{Zn}^{2+} > \text{Cu}^{2+} > \text{Ni}^{2+}$ and $\text{Cu}^{2+} > \text{Zn}^{2+} > \text{Ni}^{2+}$. Langmuir, Freundlich and Sips models proved satisfactory in describing Cu^{2+} and Ni^{2+} experimental data. Langmuir and Freundlich models describe properly the Zn^{2+} experimental data. The adsorption kinetics were fast for Cu^{2+} and Zn^{2+} . The selectivity was higher for Cu^{2+} and Zn^{2+} than for Ni^{2+} , for all the studied systems. Therefore, the synthesized zeolite 4A was confirmed to be an effective adsorbent in the removal of Cu^{2+} and Zn^{2+} from aqueous medium.

Acknowledgments

The authors would like to thank the Fundação Cearense de Apoio ao Desenvolvimento Científico e Tecnológico (FUNCAP) for the financial support. The authors also would like to thank to Laboratório de Raios-X and Professor José Marcos Sasaki for XRD analyses and Central Analítica- UFC for the SEM analysis (UFC/CT-INFRA/MCTI-SISNANO/Pró-equipamentos-CAPES).

References

- [1] D. de Quadros Melo, C.B. Vidal, A.L. da Silva, G.S.C. Raulino, A.D. da Luz, C. da Luz, P.B.A. Fachine, S.E. Mazzeto, R.F. do Nascimento, Removal of toxic metal ions using modified lignocellulosic fibers as eco-friendly biosorbents: mathematical modeling and numerical simulation, *Int. J. Civ. Environ. Eng. IJCEE-IJENS*, 15 (2015) 14–25.
- [2] M. Hong, L. Yu, Y. Wang, J. Zhang, Z. Chen, L. Dong, Q. Zan, R. Li, Heavy metal adsorption with zeolites: the role of hierarchical pore architecture, *Chem. Eng. J.*, 359 (2019) 363–372.
- [3] P. Punrattanasin, P. Sariem, Adsorption of copper, zinc, and nickel using loesses as adsorbents by column studies, *Pol. J. Environ. Stud.*, 24 (2015) 1267–1275.
- [4] S. Zhang, M. Cui, J. Chen, Z. Ding, X. Wang, Y. Mu, C. Meng, Modification of synthetic zeolite X by thiourea and its adsorption for Cd(II), *Mater. Lett.*, 236 (2019) 233–235.
- [5] D. de Quadros Melo, V. de Oliveira Sousa Neto, F.C. de Freitas Barros, G.S.C. Raulino, C.B. Vidal, R.F. do Nascimento, Chemical modifications of lignocellulosic materials and their application for removal of cations and anions from aqueous solutions, *J. Appl. Polym. Sci.*, 133 (2016) 43286, doi: 10.1002/app.43286.
- [6] D. de Quadros Melo, C.B. Vidal, A.L. da Silva, R.N.P. Teixeira, G.S.C. Raulino, T.C. Medeiros, P.B.A. Fachine, S.E. Mazzeto, D. De Keukeleire, R.F. Nascimento, Removal of Cd^{2+} , Cu^{2+} , Ni^{2+} , and Pb^{2+} ions from aqueous solutions using tururi fibers as an adsorbent, *J. Appl. Polym. Sci.*, 131 (2014) 40883, doi: 10.1002/app.40883.
- [7] G.S.C. Raulino, L.S. da Silva, C.B. Vidal, E. de Sousa Almeida, D. de Quadros Melo, R.F. do Nascimento, Role of surface chemistry and morphology in the reactive adsorption of metal ions on acid modified dry bean pods (*Phaseolus vulgaris* L.) organic polymers, *J. Appl. Polym. Sci.*, 135 (2018) 45879, doi: 10.1002/app.45879.
- [8] A.M. Arquilada, C.J. Ilano, J.M.F. Precious Pineda, A. Cid-Andres, Adsorption studies of heavy metals and dyes using corn cob: a review, *Global Sci. J.*, 6 (2018) 343–376.
- [9] S.A. Moreira, D. de Quadros Melo, A.C.A. de Lima, F.W. Sousa, A.G. Oliveira, A.H.B. Oliveira, R.F. Nascimento, Removal of

- Ni²⁺, Cu²⁺, Zn²⁺, Cd²⁺ and Pb²⁺ ions from aqueous solutions using cashew peduncle bagasse as an eco-friendly biosorbent, *Desal. Water Treat.*, 57 (2016) 10462–10475.
- [10] F.W. Sousa, A.G. Oliveira, J.P. Ribeiro, D. De Keukeleire, A.F. Sousa, R.F. Nascimento, Single and multielementary isotherms of toxic metals in aqueous solution using treated coconut shell powder, *Desal. Water Treat.*, 36 (2011) 289–296.
- [11] D. de Quadros Melo, C.B. Vidal, T.C. Medeiros, G.S.C. Raulino, A. Dervanoski, M. do Carmo Pinheiro, R.F. do Nascimento, Biosorption of metal ions using a low cost modified adsorbent (*Mauritia flexuosa*): experimental design and mathematical modeling, *Environ. Technol.*, 37 (2016) 2157–2171.
- [12] B.G.P. Bezerra, A. Parodia, D.R. da Silva, S.B.C. Pergher, Cleaning produced water: a study of cation and anion removal using different adsorbents, *J. Environ. Chem. Eng.*, 7 (2019) 103006, doi: 10.1016/j.jece.2019.103006.
- [13] C.B. Vidal, B.A. dos Santos, A.M.M. França, R.A. Bessa, A.R. Loiola, R.F. do Nascimento, Magnetite-Zeolite Nanocomposite Applied to Remediation of Polluted Aquatic Environments, R.F. do Nascimento, V. de Oliveira Sousa Neto, P.B.A. Fachine, P. de Tarso Cavalcante Freire, Eds., *Nanomaterials and Nanotechnology: Biomedical, Environmental, and Industrial Applications*, Springer, Singapore, 2021, pp. 69–94.
- [14] F.W. Sousa, A.G. Oliveira, J.P. Ribeiro, M.F. Rosa, D. Keukeleire, R.F. Nascimento, Green coconut shells applied as adsorbent for removal of toxic metal ions using fixed-bed column technology, *J. Environ. Manage.*, 91 (2010) 1634–1640.
- [15] G.S.C. Raulino, C.B. Vidal, A.C.A. Lima, D.Q. Melo, J.T. Oliveira, R.F. Nascimento, Treatment influence on green coconut shells for removal of metal ions: pilot-scale fixed-bed column, *Environ. Technol.*, 35 (2014) 1711–1720.
- [16] F.W. Sousa, M.J. Sousa, I.R.N. Oliveira, A.G. Oliveira, R.M. Cavalcante, P.B.A. Fachine, V.O.S. Neto, D. de Keukeleire, R.F. Nascimento, Evaluation of a low-cost adsorbent for removal of toxic metal ions from wastewater of an electroplating factory, *J. Environ. Manage.*, 90 (2009) 3340–3344.
- [17] H.B. Hadjtaief, A. Sdiri, W. Ltaief, P. Da Costa, M.E. Gálvez, M.B. Zina, Efficient removal of cadmium and 2-chlorophenol in aqueous systems by natural clay: adsorption and photo-Fenton degradation processes, *C.R. Chim.*, 21 (2018) 253–262.
- [18] C.B. Vidal, G.S. Raulino, A.L. Barros, A.C.A. Lima, J.P. Ribeiro, M.J.R. Pires, R.F. Nascimento, BTEX removal from aqueous solutions by HDTMA-modified Y zeolite, *J. Environ. Manage.*, 112 (2012) 178–185.
- [19] W. Yang, Q. Tang, J. Wei, Y. Ran, L. Chai, H. Wang, Enhanced removal of Cd(II) and Pb(II) by composites of mesoporous carbon stabilized alumina, *Appl. Surf. Sci.*, 369 (2016) 215–223.
- [20] M. Sharma, J. Singh, S. Hazra, S. Basu, Adsorption of heavy metal ions by mesoporous ZnO and TiO₂@ZnO monoliths: adsorption and kinetic studies, *Microchem. J.*, 145 (2019) 105–112.
- [21] F. Ciesielczyk, P. Bartczak, K. Wieszczycka, K. Siwińska-Stefańska, M. Nowacka, T. Jesionowski, Adsorption of Ni(II) from model solutions using co-precipitated inorganic oxides, *Adsorption*, 19 (2013) 423–434.
- [22] L.S. Silva, G.S.C. Raulino, C.B. Vidal, M.J.R. Pires, R.F. Nascimento, Peculiar properties of LTA/FAU synthetic composite zeolite and its effect on Cu²⁺ adsorption: factorial experimental design, *Desal. Water Treat.*, 107 (2018) 223–231.
- [23] Z. Wang, K. Tan, J. Cai, S. Hou, Y. Wang, P. Jiang, M. Liang, Silica oxide encapsulated natural zeolite for high efficiency removal of low concentration heavy metals in water, *Colloids Surf., A*, 561 (2019) 388–394.
- [24] D. Czarna, P. Baran, P. Kunecki, R. Panek, R. Żmuda, M. Wdowin, Synthetic zeolites as potential sorbents of mercury from wastewater occurring during wet FGD processes of flue gas, *J. Cleaner Prod.*, 172 (2018) 2636–2645.
- [25] R.J. Costa, E.A.S. Castro, J.R.S. Politi, R. Gargano, J.B.L. Martins, Methanol, ethanol, propanol, and butanol adsorption on H-ZSM-5 zeolite: an ONIOM study, *J. Mol. Model.*, 25 (2019) 34, doi: 10.1007/s00894-018-3894-2.
- [26] L.R. Rad, A. Momeni, B.F. Ghazani, M. Irani, M. Mahmoudi, B. Noghreh, Removal of Ni²⁺ and Cd²⁺ ions from aqueous solutions using electrospun PVA/zeolite nanofibrous adsorbent, *Chem. Eng. J.*, 256 (2014) 119–127.
- [27] R. de Andrade Bessa, L. de Sousa Costa, C.P. Oliveira, F. Bohn, R.F. do Nascimento, J.M. Sasaki, A.R. Loiola, Kaolin-based magnetic zeolites A and P as water softeners, *Microporous Mesoporous Mater.*, 245 (2017) 64–72.
- [28] M. Khodadadi, A. Malekpour, M. Ansaritabar, Removal of Pb(II) and Cu(II) from aqueous solutions by NaA zeolite coated magnetic nanoparticles and optimization of method using experimental design, *Microporous Mesoporous Mater.*, 248 (2017) 256–265.
- [29] Z. Ezzeddine, I. Batonneau-Gener, Y. Pouilloux, H. Hamad, Z. Saad, Synthetic NaA zeolite as a very efficient heavy metals sorbent in batch and dynamic conditions, *Colloids Interfaces*, 2 (2018) 22, doi: 10.3390/colloids2020022.
- [30] X. Shen, G. Qiu, C. Yue, M. Guo, M. Zhang, Multiple copper adsorption and regeneration by zeolite 4A synthesized from bauxite tailings, *Environ. Sci. Pollut. Res.*, 24 (2017) 21829–21835.
- [31] R.W. Thompson, M.J. Huber, Analysis of the growth of molecular sieve zeolite NaA in a batch precipitation system, *J. Cryst. Growth*, 56 (1982) 711–722.
- [32] S. Malamis, E. Katsou, A review on zinc and nickel adsorption on natural and modified zeolite, bentonite and vermiculite: examination of process parameters, kinetics and isotherms, *J. Hazard. Mater.*, 252 (2013) 428–461.
- [33] S. He, Y. Li, L. Weng, J. Wang, J. He, Y. Liu, K. Zhang, Q. Wu, Y. Zhang, Z. Zhang, Competitive adsorption of Cd²⁺, Pb²⁺ and Ni²⁺ onto Fe³⁺-modified argillaceous limestone: influence of pH, ionic strength and natural organic matters, *Sci. Total Environ.*, 637 (2018) 69–78.
- [34] G.J. Joshiba, P.S. Kumar, F.C. Christopher, G. Pooja, V.V. Kumar, Fabrication of novel amine-functionalized magnetic silica nanoparticles for toxic metals: kinetic and isotherm modeling, *Environ. Sci. Pollut. Res.*, 27 (2020) 27202–27210.
- [35] X. An, L. Zhang, Y. He, W. Zhu, Y. Luo, Kinetic, isotherm, and thermodynamic studies of Cr(VI) removal from aqueous solution using mesoporous silica materials prepared by fly ash, *Can. J. Chem. Eng.*, 98 (2020) 1825–1834.
- [36] C.B. Vidal, D.Q. Melo, G.S.C. Raulino, A.D. da Luz, C. da Luz, R.F. Nascimento, Multielement adsorption of metal ions using Tururi fibers (*Manicaria Saccifera*): experiments, mathematical modeling and numerical simulation, *Desal. Water Treat.*, 57 (2016) 9001–9008.
- [37] C.B. Vidal, A.V. Feitosa, G.P. Pessoa, G.S.C. Raulino, A.G. Oliveira, A.B. dos Santos, R.F. Nascimento, Polymeric and silica sorbents on endocrine disruptors determination, *Desal. Water Treat.*, 54 (2015) 156–165.
- [38] I. Langmuir, The dissociation of hydrogen into atoms, *J. Am. Chem. Soc.*, 34 (1912) 860–877.
- [39] G. McKay, Use of Adsorbents for the Removal of Pollutants from Wastewater, CRC Press, New York, 1995.
- [40] R. Sips, On the structure of a catalyst surface, *J. Chem. Phys.*, 16 (1948) 490–495.
- [41] K.K.H. Choy, J.F. Porter, G. McKay, E. Data, Langmuir isotherm models applied to the multicomponent sorption of acid dyes from effluent onto activated carbon, *J. Chem. Eng. Data*, 45 (2000) 575–584.
- [42] D.M. Ruthven, Principles of Adsorption and Adsorption Processes, John Wiley & Sons, New York, 1984.
- [43] R.M. Galante, G.N. Mara, R. Machado, Modelagem e simulação do processo de extração de inulina a partir do alho (*Allium sativum* L. var. chonan) em batelada para diferentes temperaturas, *Braz. J. Food Technol.*, 13 (2010) 174–181.
- [44] D.O. Cooney, Adsorption Design for Wastewater Treatment, CRC Press, United States, 1998.
- [45] gPROMS, gPROMS User Guide: Advanced Process Modelling and Simulation, Process Systems Enterprise, 2006.
- [46] M.Š. Ivanović, I. Smičiklas, S. Pejanović, Analysis and comparison of mass transfer phenomena related to Cu²⁺ sorption by hydroxyapatite and zeolite, *Chem. Eng. J.*, 223 (2013) 833–843.
- [47] F.-Q. An, H.-F. Li, X.-D. Guo, B.-J. Gao, T.-P. Hu, J.-F. Gao, Novel ionic surface imprinting technology: design and application for

- selectively recognizing heavy metal ions, *RSC Adv.*, 9 (2019) 2431–2440.
- [48] B. Anna, M. Kleopas, S. Constantine, F. Anestis, B. Maria, Adsorption of Cd(II), Cu(II), Ni(II) and Pb(II) onto natural bentonite: study in mono- and multi-metal systems, *Environ. Earth Sci.*, 73 (2015) 5435–5444.
- [49] L. Sellaoui, F.E. Soetaredjo, S. Ismadji, Y. Benguerba, G.L. Dotto, A. Bonilla-Petriciolet, A.E. Rodrigues, A.B. Lamine, A. Erto, Equilibrium study of single and binary adsorption of lead and mercury on bentonite-alginate composite: experiments and application of two theoretical approaches, *J. Mol. Liq.*, 253 (2018) 160–168.
- [50] Liu, B. Lian, Non-competitive and competitive adsorption of Cd²⁺, Ni²⁺, and Cu²⁺ by biogenic vaterite, *Sci. Total Environ.*, 659 (2019) 122–130.
- [51] J.M. Adams, D.A. Haselden, A.W. Hewat, The structure of dehydrated Na zeolite A (Si/Al = 1.09) by neutron profile refinement, *J. Solid State Chem.*, 44 (1982) 245–253.
- [52] N.M. Musyoka, L.F. Petrik, E. Hums, A. Kuhnt, W. Schwieger, Thermal stability studies of zeolites A and X synthesized from South African coal fly ash, *Res. Chem. Intermed.*, 41 (2015) 575–582.
- [53] A.R. Loiola, J.C.R.A. Andrade, J.M. Sasaki, L.R.D. da Silva, Structural analysis of zeolite NaA synthesized by a cost-effective hydrothermal method using kaolin and its use as water softener, *J. Colloid Interface Sci.*, 367 (2012) 34–39.
- [54] M. Anbia, E. Koohsaryan, A. Borhani, Novel hydrothermal synthesis of hierarchically-structured zeolite LTA microspheres, *Mater. Chem. Phys.*, 193 (2017) 380–390.
- [55] L. Yang, X. Qian, P. Yuan, H. Bai, T. Miki, F. Men, H. Li, T. Nagasaka, Green synthesis of zeolite 4A using fly ash fused with synergism of NaOH and Na₂CO₃, *J. Cleaner Prod.*, 212 (2019) 250–260.
- [56] X. Ren, L. Xiao, R. Qu, S. Liu, D. Ye, H. Song, W. Wu, C. Zheng, X. Wu, X. Gao, Synthesis and characterization of a single phase zeolite A using coal fly ash, *RSC Adv.*, 8 (2018) 42200–42209.
- [57] A.E. Burakov, E.V. Galunin, I.V. Burakova, A.E. Kucherova, S. Agarwal, A.G. Tkachev, V.K. Gupta, Adsorption of heavy metals on conventional and nanostructured materials for wastewater treatment purposes: a review, *Ecotoxicol. Environ. Saf.*, 148 (2018) 702–712.
- [58] Renu, M. Agarwal, K. Singh, Heavy metal removal from wastewater using various adsorbents: a review, *J. Water Reuse Desal.*, 7 (2017) 387–419.
- [59] S. Lata, P.K. Singh, S.R. Samadder, Regeneration of adsorbents and recovery of heavy metals: a review, *Int. J. Environ. Sci. Technol.*, 12 (2015) 1461–1478.
- [60] K.S. Hui, C.Y.H. Chao, S.C. Kot, Removal of mixed heavy metal ions in wastewater by zeolite 4A and residual products from recycled coal fly ash, *J. Hazard. Mater.*, 127 (2005) 89–101.
- [61] S. Xing, M. Zhao, Z. Ma, Removal of heavy metal ions from aqueous solution using red loess as an adsorbent, *J. Environ. Sci.*, 23 (2011) 1497–1502.
- [62] G. Chen, L. Shi, Removal of Cd(II) and Pb(II) ions from natural water using a low-cost synthetic mineral: behavior and mechanisms, *RSC Adv.*, 7 (2017) 43445–43454.
- [63] B. Das, Equilibrium and kinetic studies on adsorption of copper from aqueous solution by neem (*Azadirachta indica*) bark powder, *Int. J. Sci. Res. Sci. Technol.*, 4 (2018) 290–298.
- [64] J. Perić, M. Trgo, N. Vukojević Medvidović, Removal of zinc, copper and lead by natural zeolite—a comparison of adsorption isotherms, *Water Res.*, 38 (2004) 1893–1899.
- [65] B.H. Hameed, I.A.W. Tan, A.L. Ahmad, Adsorption isotherm, kinetic modeling and mechanism of 2,4,6-trichlorophenol on coconut husk-based activated carbon, *Chem. Eng. J.*, 144 (2008) 235–244.
- [66] K. He, Y. Chen, Z. Tang, Y. Hu, Removal of heavy metal ions from aqueous solution by zeolite synthesized from fly ash, *Environ. Sci. Pollut. Res.*, 23 (2016) 2778–2788.
- [67] E.R. Nightingale Jr., Phenomenological theory of ion solvation. Effective radii of hydrated ions, *J. Phys. Chem.*, 63 (1959) 1381–1387.
- [68] M.J. Moon, M.S. Jhon, The studies on the hydration energy and water structures in dilute aqueous solution, *B. Chem. Soc. Jpn.*, 59 (1986) 1215–1222.
- [69] D.W. Barnum, Hydrolysis of cations. Formation constants and standard free energies of formation of hydroxy complexes, *Inorg. Chem.*, 22 (1983) 2297–2305.
- [70] M.W. Munthali, E. Johan, N. Matsue, Proton adsorption selectivity of zeolites in aqueous media: effect of exchangeable cation species of zeolites, *Environment*, 2 (2015) 91–104.
- [71] L. Mihaly-Cozmata, A. Mihaly-Cozmata, A. Peter, C. Nicula, H. Tutu, D. Silipas, E. Indrea, Adsorption of heavy metal cations by Na-clinoptilolite: equilibrium and selectivity studies, *J. Environ. Manage.*, 137 (2014) 69–80.
- [72] A.R.A. Usman, The relative adsorption selectivities of Pb, Cu, Zn, Cd and Ni by soils developed on shale in New Valley, Egypt, *Geoderma*, 144 (2008) 334–343.
- [73] R.O. James, T.W. Healy, Adsorption of hydrolyzable metal ions at the oxide–water interface. III. A thermodynamic model of adsorption, *J. Colloid Interface Sci.*, 40 (1972) 65–81.
- [74] T.C. Nguyen, P. Loganathan, T.V. Nguyen, J. Kandasamy, R. Naidu, S. Vigneswaran, Adsorptive removal of five heavy metals from water using blast furnace slag and fly ash, *Environ. Sci. Pollut. Res.*, 25 (2018) 20430–20438.
- [75] M. de S. Gama, F.M.T. Luna, J.Q. Albarelli, M.M. Beppu, R.S. Vieira, Adsorption of copper on glass beads coated with chitosan: stirred batch and fixed bed analysis, *Can. J. Chem. Eng.*, 95 (2017) 1164–1170.
- [76] Y. Onal, C. Akmil-Başar, Ç. Sarıcı-Özdemir, Investigation kinetics mechanisms of adsorption malachite green onto activated carbon, *J. Hazard. Mater.*, 146 (2007) 194–203.
- [77] K.V. Kumar, V. Ramamurthi, S. Sivanesan, Biosorption of malachite green, a cationic dye onto *Pithophora* sp., a fresh water algae, *Dyes Pigm.*, 69 (2006) 102–107.
- [78] A.E. Ofomaja, Intraparticle diffusion process for lead(II) biosorption onto mansonia wood sawdust, *Bioresour. Technol.*, 101 (2010) 5868–5876.
- [79] K.K.H. Choy, D.C.K. Ko, C.W. Cheung, J.F. Porter, G. McKay, Film and intraparticle mass transfer during the adsorption of metal ions onto bone char, *J. Colloid Interface Sci.*, 271 (2004) 284–295.
- [80] U.K. Saha, S. Taniguchi, K. Sakurai, Simultaneous adsorption of cadmium, zinc, and lead on hydroxylaluminum- and hydroxylaluminosilicate-montmorillonite complexes, *Soil Sci. Soc. Am. J.*, 66 (2002) 117–128.
- [81] M. Majdan, S. Pikus, M. Kowalska-Ternes, A. Gładysz-Płaska, P. Staszczuk, L. Fuks, H. Skrzypek, Equilibrium study of selected divalent d-electron metals adsorption on A-type zeolite, *J. Colloid Interface Sci.*, 262 (2003) 321–330.
- [82] X. Liu, R. Tian, W. Ding, Y. He, H. Li, Adsorption selectivity of heavy metals by Na-clinoptilolite in aqueous solutions, *Adsorption*, 25 (2019) 747–755.
- [83] Z. Ezzeddine, I.B. Gener, Y. Pouilloux, Cation exchange mechanism of divalent metals ions in synthetic NaX and LTA zeolites: efficiency and selectivity, *Eur. Chem. Bull.*, 7 (2018) 93–98.
- [84] K. Nakamoto, M. Ohshiro, T. Kobayashi, Mordenite zeolite–polyethersulfone composite fibers developed for decontamination of heavy metal ions, *J. Environ. Chem. Eng.*, 5 (2017) 513–525.
- [85] E.A. Ayuso, A.G. Sánchez, X. Querol, Purification of metal electroplating waste waters using zeolites, *Water Res.*, 37 (2003) 4855–4862.
- [86] A. Regti, A. El Kassimi, M.R. Laamari, M. El Haddad, Competitive adsorption and optimization of binary mixture of textile dyes: a factorial design analysis, *J. Assoc. Arab Univ. Basic Appl. Sci.*, 24 (2017) 1–9.
- [87] A. Erto, F. Di Natale, D. Musmarra, A. Lancia, Modeling of single and competitive adsorption of cadmium and zinc onto activated carbon, *Adsorption*, 21 (2015) 611–621.